Quantized Majorana conductance

Zhang, Hao; Liu, Chun Xiao; Gazibegovic, Sasa; Xu, Di; Logan, John A.; Wang, Guanzhong; Van Loo, Nick; Bommer, Jouri D.S.; De Moor, Michiel W.A.; Car, Diana

DOI
10.1038/nature26142

Publication date
2018

Document Version
Accepted author manuscript

Published in
Nature

Citation (APA)
Zhang, H., Liu, C. X., Gazibegovic, S., Xu, D., Logan, J. A., Wang, G., Van Loo, N., Bommer, J. D. S., De Moor, M. W. A., Car, D., Op Het Veld, R. L. M., Van Veldhoven, P. J., Koelling, S., Verheijen, M. A., Pendharkar, M., Pennachio, D. J., Shojaei, B., Lee, J. S., Palmstrøm, C. J., ... Kouwenhoven, L. P. (2018). Quantized Majorana conductance. *Nature*, *556*(7699), 74-79. https://doi.org/10.1038/nature26142

Quantized Majorana Conductance

Hao Zhang, Di Xu, Guanzhong Wang, Nick van Loo, Jouri D.S. Bommer, Michiel W.A. de Moor, Leo P. Kouwenhoven [1]

[1] *QuTech and Kavli Institute of NanoScience, Delft University of Technology, 2600 GA Delft, the Netherlands*
Microsoft Station Q Delft, 2600 GA Delft, The Netherlands

Chun-Xiao Liu, S. Das Sarma

Condensed Matter Theory Center and Joint Quantum Institute, Department of Physics, University of Maryland, College Park, Maryland 20742, USA

John A. Logan[sb1], Mihir Pendharkar[sb2], Daniel J. Pennachio[sb1], Borzoyeh Shojaei[sb1,sb3], Joon Sue Lee[sb3], Chris J. Palmstrøm[sb1,sb2,sb3]

[sb1] *Materials Engineering, University of California Santa Barbara, Santa Barbara, CA, USA 93106*
[sb2]*Electrical and Computer Engineering, University of California Santa Barbara, Santa Barbara, CA, USA 93106*
[sb3] *California NanoSystems Institute, University of California Santa* Materials, *Santa Barbara, CA, USA 93106*

Sasa Gazibegovic,1,2, Diana Car,1,2, Roy L. M. Op het Veld,1,2 Petrus J. van Veldhoven,2 Sebastian Koelling,2 Marcel A. Verheijen,2,7 Erik P.A.M. Bakkers1,2

1 QuTech and Kavli Institute of NanoScience, Delft University of Technology, 2600 GA Delft, the Netherlands
2 Department of Applied Physics, Eindhoven University of Technology, 5600 MB Eindhoven, the Netherlands
7 Philips Innovation Services Eindhoven, High Tech Campus 11, 5656AE Eindhoven, the Netherlands

Majorana zero-modes hold great promise for topological quantum computing. Tunnelling spectroscopy in electrical transport is the primary tool to identify the presence of Majorana zero-modes, for instance as a zero-bias peak (ZBP) in differential-conductance. The Majorana ZBP-height is predicted to be quantized at the universal conductance value of $2e^2/h$ *at zero temperature*. Interestingly, this quantization is a direct consequence of the famous Majorana symmetry, "particle equals antiparticle". The Majorana symmetry protects the quantization against disorder, interactions, and variations in the tunnel coupling. Previous experiments, however, have shown ZBPs much smaller than $2e^2/h$, with a recent observation of a peak-height close to $2e^2/h$. Here, we report a quantized conductance *plateau* at $2e^2/h$ in the zero-bias conductance measured in InSb semiconductor nanowires covered with an Al superconducting shell. Our ZBP-height remains constant despite changing parameters such as the magnetic field and tunnel coupling, i.e. a quantized conductance plateau. We distinguish this quantized Majorana peak from possible non-Majorana origins, by investigating its robustness on electric and magnetic fields as well as its temperature dependence. A fully-developed quantized plateau is a necessary step towards demonstrating non-Abelian braiding statistics with Majorana zero-modes.

A semiconductor nanowire coupled to a superconductor can be tuned into a topological superconductor with two Majorana zero-modes localized at the wire ends[1-3]. Tunnelling into a Majorana mode will show a zero-energy state in the tunnelling density-of-states, i.e. a zero-bias peak (ZBP) in the differential conductance (dI/dV)[4,5]. This tunnelling process is a so-called Andreev reflection, where an incoming electron is reflected as a hole. Particle-hole symmetry dictates that the zero-energy tunnelling amplitudes of electrons and holes are equal, resulting in a perfect resonant transmission with a ZBP-height quantized at $2e^2/h$[6-8], irrespective of the precise

tunnelling strength[9]. The Majorana-nature of this perfect Andreev reflection is a direct result of the well-known Majorana symmetry property “particle equals antiparticle”[10,11].

Such a predicted robust conductance quantization has not yet been observed[4,5,12-14]. Instead, most of the ZBPs have a height significantly less than $2e^2/h$. This discrepancy was first explained by thermal averaging[15-18]. This explanation, however, does not hold when the peak-width exceeds the thermal broadening (~$3.5k_BT$)[12,13]. In that case, other averaging mechanisms, such as dissipation[19], have been invoked. The main source of dissipation is a finite quasi-particle density-of-states within the superconducting gap, often referred to as a ‘soft gap’. Substantial advances have been achieved in ‘hardening’ the gap by improving materials quality, eliminating disorder and interface roughness[20,21], and better control during device processing[22,23], all guided by a more detailed theoretical understanding[24]. We have recently solved all these dissipation and disorder issues[21], and here we report the resulting improvements in electrical transport leading to the so-far elusive quantization of the Majorana ZBP.

Fig.1a shows a micrograph of a fabricated device and schematics of the measurement set-up. An InSb nanowire (grey) is partially covered (two out of six facets) by a thin superconducting Al shell (green)[21]. The ‘tunnel-gates’ (coral red) are used to induce a tunnel barrier in the non-covered segment between the left electrical contact (yellow) and the Al shell. The right contact is used to drain the current to ground. The chemical potential in the segment proximitized by Al can be tuned by applying voltages to the two long ‘super-gates’ (purple).

Transport spectroscopy is shown in Fig.1b displaying dI/dV as a function of voltage bias, V, and magnetic field, B (aligned with the nanowire axis), while applying fixed voltages to the tunnel- and super-gates. As B increases, two levels detach from the gap edge (at ~0.2 meV), merge at zero bias, and form a robust ZBP. This is consistent with the Majorana theory: a ZBP is formed after the Zeeman energy closes the trivial superconducting gap and re-opens a topological

gap[2,3]. The gap re-opening is not visible in a measurement of the local density-of-states since the tunnel coupling to these bulk states is small[25]. Moreover, the finite length of the proximitized segment (~1.2 μm) results in discrete energy states, turning the trivial-to-topological phase transition into a smooth cross-over[26]. Fig.1c shows two line-cuts from Fig.1b extracted at 0 and 0.88 T. Importantly, the height of the ZBP reaches the quantized value of $2e^2/h$. The line-cut at zero-bias in the lower panel of Fig.1b shows that the ZBP-height remains close to $2e^2/h$ over a sizable range in B-field (0.75 - 0.92 T). Beyond this range, the height drops, most likely caused by a closure of the superconducting gap in the bulk Al contact.

We note that the sub-gap conductance at $B = 0$ (black curve, left panel, Fig.1c) is not completely suppressed down to zero, reminiscent of a soft gap. In this case, this finite sub-gap conductance, however, does not reflect any finite sub-gap density-of-states in the proximitized wire. It arises from Andreev reflection (i.e. transport by dissipationless Cooper pairs) due to a high tunnelling transmission, which is evident from the above-gap conductance (dI/dV for $V > 0.2$ V) being larger than e^2/h. Since this softness does not result from dissipation, the Majorana peak-height should still reach the quantized value[27]. In Extended Data Fig. 1, we show that this device tuned into a low transmission regime, where dI/dV does reflect the density-of-states, indeed displays a hard gap. For further understanding we use experimental parameters in a theoretical Majorana nanowire model[28] (see Methods for more information). Fig. 1d shows a simulation with two line-cuts in Fig. 1c (right panel). Besides the ZBP, other discrete sub-gap states are visible, which are due to the finite wire length. Such discrete lines are only faintly resolved in the experimental panels of Fig. 1b. Overall, we find good qualitative agreement between the experimental and simulation panels in Fig. 1b and 1d. We note that an exact quantitative agreement is not feasible since the precise experimental values for the parameters going into the theory (e.g. chemical potential, tunnel coupling, Zeeman splitting, spin-orbit coupling, etc.) are unknown for our hybrid wire-superconductor structure.

Next, we fix B at 0.8 T and investigate the robustness of the quantized ZBP against variations in the transmission by varying the voltage on the tunnel-gate. Fig. 2a shows dI/dV while varying V and tunnel-gate voltage. Fig. 2b shows that the ZBP-height remains close to the quantized value. Importantly, the above-gap conductance measured at $|V| = 0.2$ meV varies by more than 50% (Fig. 2c and 2d), implying that the transmission is changing significantly over this range while the ZBP remains quantized. Note that the minor conductance switches in Fig. 2a-c are due to unstable jumps of trapped charges in the surroundings.

Fig. 2d (red curves) shows several line-cuts of the quantized ZBP. The extracted height and width are plotted in Fig. 2e (upper panel) as a function of above-gap conductance $G_N = T \times e^2/h$ where T is the transmission probability for a spin-resolved channel. While the ZBP-width does change with G_N, the quantized height remains unaffected. Note that the ZBP-width ranges from ~50 to ~100 μeV, which is significantly wider than the thermal width ~6 μeV at 20 mK. The ZBP-width is thus broadened by tunnel coupling, instead of thermal broadening, i.e. fulfilling a necessary condition to observe a quantized Majorana peak. In Extended Data Fig. 2, we show that in the low transmission regime where thermal broadening dominates over tunnel broadening, the ZBP-height drops below $2e^2/h$[15-18]. We emphasize that the robustness of the ZBP quantization to a variation in the tunnel barrier is an important finding of our work.

A more negative tunnel-gate voltage (< -8 V) eventually splits the ZBP, which may be explained by an overlapping of the two localized Majorana wave-functions from the two wire ends. The tunnel-gate not only tunes the transmission of the barrier, but also influences the potential profile in the proximitized wire part near the tunnel barrier. A more negative gate voltage effectively pushes the nearby Majorana mode away, towards the remote Majorana on the other end of the wire, thus reducing the length of the effective topological wire. This leads to the wave-function overlap between the two Majoranas, causing the ZBP to split[16] (black curves in Fig. 2d). This splitting is also captured in our simulations shown in Fig. 2f, where we have checked that the

splitting originates from Majorana wave-function overlap. Note that the simulated ZBP-height (red curve in middle panel in Fig. 2f) remains close to the $2e^2/h$ plateau over a large range, while the above-gap conductance (black curve in lower panel in Fig. 2f) changes substantially. Also, the height and width dependence in the simulation is in qualitative agreement with our experimental observation (Fig. 2e). To complete the comparison, we show in Fig. 2g the simulated line-cuts of several quantized ZBP's (red curves) and split peaks (black curves), consistent with the experimental data in Fig. 2d.

Pushing Majoranas toward each other is one mechanism for splitting. Another way is by changing the chemical potential through the transition from a topological to a trivial phase[2,3]—the topological quantum phase transition from the trivial to the topological phase can be equivalently caused by tuning either the Zeeman energy (i.e. the magnetic field) or the chemical potential. Splitting at the phase transition occurs since the Majorana wave-functions start to spread out over the entire wire length. For long wires the transition is abrupt, whereas in shorter wires a smooth transition is expected[26]. We investigate the dependence of the quantized ZBP on chemical potential by varying the voltage on the super-gate. Fig. 3a shows a nearly-quantized ZBP that remains non-split over a large range in super-gate voltage. More positive voltage applied to the super-gates corresponds to a higher chemical potential, and eventually we find a ZBP-splitting (> -5 V) and consequently a suppression of the zero-bias conductance below the quantized value. Although the relation between gate voltage and chemical potential is unknown in our devices, this splitting suggests a transition to the trivial phase caused by a tuning of the chemical potential induced by the changing super-gate voltage.

In a lower *B*-field and different gate settings (Fig. 3b), the splitting of the quantized ZBP shows oscillatory behaviour as a function of the super-gate voltage. The five line-cuts on the right panel highlight this back-and-forth behaviour between quantized and suppressed ZBPs.

Remarkably, the ZBP-height comes back up to the quantized value and, importantly, does not cross through it.

We find similar behaviour in the theoretical simulations of Fig. 3c. In these simulations we have confirmed that for the chosen parameters, the Majorana wave-functions oscillate in their overlap, thus giving rise to the back-and-forth behaviour of quantized and split ZBPs[29]. In the experiment it may also be that non-homogeneity, possibly somewhere in the middle of the wire, causes overlap of Majorana wave-functions. Again, we note that the conversion from gate voltage to chemical potential is unknown, preventing a direct quantitative comparison between experiment and simulation.

To demonstrate the reproducibility of ZBP quantization, we show in Fig. 4a the quantized ZBP data from a second device. In this second device the length of the proximitized section is ~0.9 μm, which is ~0.3 μm shorter than the previous device. This second device allows to transmit more than one channel through the tunnel barrier, which we deduce from the above-gap conductance value (Fig. 4b, lower panel, black curve) exceeding e^2/h for voltages larger than ~ -0.55 V on the tunnel-gates. Correspondingly, the zero-bias conductance can now exceed $2e^2/h$ (Fig. 4b, middle panel) for such an open tunnel barrier[9]. We note that tunnelling through the second channel in the barrier region results in an additional background conductance, thus leading to the zero-bias conductance rising above $2e^2/h$. We find, however, from a rough estimate of this background contribution that the net ZBP-height (above background) never exceeds $2e^2/h$, consistent with Majorana theory[9].

We next fix the *B*-field and study temperature dependence. Fig. 4c shows a line-cut of this quantized ZBP from Fig. 4a. First, the base temperature trace in Fig. 4c (red data points) fits well to a Lorentzian line-shape with 20 mK thermal broadening, expected for Majoranas as well as for any type of resonant transmission. The ZBP temperature dependence is shown in line traces in

Fig. 4d and in colour scale in Fig. 4e (with the corresponding simulation in the lower panel of 4e). Fig. 4f shows the extracted ZBP-height and ZBP-width (i.e. full-width-half-maximum, FWHM) from both the experimental and simulational traces. At low temperatures, the ZBP-width (red data points) exceeds the thermal width defined as $3.5k_BT$ (blue line). In agreement with theory[15,17,30], the ZBP-height (black data points) reaches and saturates at $2e^2/h$ when the FWHM exceeds $3.5k_BT$. For higher temperatures, thermal averaging starts suppressing the ZBP-height below the quantized value. We note that the simulated data is calculated by a convolution integration of the derivative of the Fermi distribution function and the *dI/dV* trace at base temperature of 20 mK. This procedure of incorporating thermal effects holds if the temperature of the calculated *dI/dV* curve is significantly larger than base temperature (which can then be assumed to be the effective zero-temperature conductance value). Indeed, we find excellent agreement between experiment and simulation for $T > 50$ mK (Fig. 4f). See Extended Data Fig. 3 for detailed temperature dependence.

Recent theoretical work[28] has shown numerically for experimentally relevant parameters that ZBPs can also arise from local and non-topological Andreev bound states (ABS)[16,31-34]. These local ABS appear remarkably similar in tunnelling spectroscopy as the ZBPs arising from Majorana zero-modes. In a third device, we have been able to find such non-topological states by fine-tuning gate voltages. Figure 5 shows the similarities and differences between ABS and Majorana ZBPs. First of all, Fig. 5a shows a ZBP in tunnelling spectroscopy versus *B*-field. At a particular *B*-field (0.7 T, red bar) the ZBP-height reaches $2e^2/h$. In this device, we next vary the chemical potential via a voltage applied to a back-gate, showing a fairly stable (non-split) ZBP in Fig. 5b. In contrast, the ZBP is unstable against variations in tunnel-gate voltage. Fig. 5c shows that now the ZBP appears as level crossings instead of being rigidly bound to zero bias. The two different behaviours between back-gate and tunnel-gate are expected for ABSs that are localized near the tunnel barrier, as was modelled explicitly in Ref. 28 (see also Extended Data Fig. 5). Liu

et al.[28] show that local ABSs can have near-zero energy, which in a *B*-field is remarkably robust against variations in chemical potential; in our experiment tuned by the back-gate. However, this is only the case for the tunnel-gate voltage fine-tuned to level crossing points at zero bias. The local tunnel-gate and the global back-gate thus have distinguishably different effects. For the Majorana case, instead of level crossing, the ZBP should remain non-split over sizable changes in tunnel-gate voltage[13], as shown in Fig. 2a and Fig. 4b.

The second fundamental difference is that the non-topological ABS ZBP-height is not expected to be robustly quantized at $2e^2/h$[9,28]. Fig. 5d and 5e show that the ZBP-height varies smoothly as a function of the back-gate voltage without any particular feature at $2e^2/h$. Also, the ZBP-height in Fig. 5a at $2e^2/h$ is just a tuned coincidence (see Extended Data Fig. 6). Note that the ZBP line-shape or temperature dependence does not discriminate between topological and non-topological cases. Both fit a Lorentzian line-shape as shown explicitly for the non-topological ABS in Fig. 5f. Thus, the temperature dependence alone cannot distinguish a Majorana origin from ABS[14,30,31]. Only a stable quantized tunnel-conductance plateau, robust against variations in all gate voltages and magnetic field strength, can uniquely identify a topological Majorana zero-mode.

References

1 Kitaev, A. Y. Unpaired Majorana fermions in quantum wires. *Physics-Uspekhi* **44**, 131 (2001).

2 Lutchyn, R. M., Sau, J. D. & Das Sarma, S. Majorana Fermions and a Topological Phase Transition in Semiconductor-Superconductor Heterostructures. *Physical Review Letters* **105**, 077001 (2010).

3 Oreg, Y., Refael, G. & von Oppen, F. Helical Liquids and Majorana Bound States in Quantum Wires. *Physical Review Letters* **105**, 177002 (2010).

4 Mourik, V. *et al*. Signatures of Majorana Fermions in Hybrid Superconductor-Semiconductor Nanowire Devices. *Science* **336**, 1003-1007 (2012).

5 Lutchyn, R. M. *et al*. Realizing Majorana zero modes in superconductor-semiconductor heterostructures. *arXiv:1707.04899* (2017).

6 Sengupta, K., Žutić, I., Kwon, H.-J., Yakovenko, V. M. & Das Sarma, S. Midgap edge states and pairing symmetry of quasi-one-dimensional organic superconductors. *Physical Review B* **63**, 144531 (2001).

7 Law, K. T., Lee, P. A. & Ng, T. K. Majorana Fermion Induced Resonant Andreev Reflection. *Physical Review Letters* **103**, 237001 (2009).

8 Flensberg, K. Tunneling characteristics of a chain of Majorana bound states. *Physical Review B* **82**, 180516 (2010).
9 Wimmer, M., Akhmerov, A. R., Dahlhaus, J. P. & Beenakker, C. W. J. Quantum point contact as a probe of a topological superconductor. *New Journal of Physics* **13**, 053016 (2011).
10 Majorana, E. A symmetric theory of electrons and positrons. *Soryushiron Kenkyu (English translation)* **63**, 149, doi:[translation from Nuovo Cimento 14, 171 (1937)] (1981).
11 Read, N. & Green, D. Paired states of fermions in two dimensions with breaking of parity and time-reversal symmetries and the fractional quantum Hall effect. *Physical Review B* **61**, 10267-10297 (2000).
12 Deng, M. T. *et al.* Majorana bound state in a coupled quantum-dot hybrid-nanowire system. *Science* **354**, 1557 (2016).
13 Gül, Ö. *et al.* Ballistic Majorana Nanowire Devices. *Nature Nanotechnology (in Press)* (2017).
14 Nichele, F. *et al.* Scaling of Majorana Zero-Bias Conductance Peaks. *Physical Review Letters* **119**, 136803 (2017).
15 Pientka, F., Kells, G., Romito, A., Brouwer, P. W. & von Oppen, F. Enhanced Zero-Bias Majorana Peak in the Differential Tunneling Conductance of Disordered Multisubband Quantum-Wire/Superconductor Junctions. *Physical Review Letters* **109**, 227006 (2012).
16 Prada, E., San-Jose, P. & Aguado, R. Transport spectroscopy of NS nanowire junctions with Majorana fermions. *Physical Review B* **86**, 180503 (2012).
17 Lin, C.-H., Sau, J. D. & Das Sarma, S. Zero-bias conductance peak in Majorana wires made of semiconductor/superconductor hybrid structures. *Physical Review B* **86**, 224511 (2012).
18 Rainis, D., Trifunovic, L., Klinovaja, J. & Loss, D. Towards a realistic transport modeling in a superconducting nanowire with Majorana fermions. *Physical Review B* **87**, 024515 (2013).
19 Liu, C.-X., Sau, J. D. & Das Sarma, S. Role of dissipation in realistic Majorana nanowires. *Physical Review B* **95**, 054502 (2017).
20 Krogstrup, P. *et al.* Epitaxy of semiconductor–superconductor nanowires. *Nat Mater* **14**, 400-406 (2015).
21 Gazibegovic, S. *et al.* Epitaxy of advanced nanowire quantum devices. *Nature* **548**, 434-438 (2017).
22 Gül, Ö. *et al.* Hard Superconducting Gap in InSb Nanowires. *Nano Letters* **17**, 2690-2696 (2017).
23 Zhang, H. *et al.* Ballistic superconductivity in semiconductor nanowires. *Nature Communications* **8**, 16025 (2017).
24 Takei, S., Fregoso, B. M., Hui, H.-Y., Lobos, A. M. & Das Sarma, S. Soft Superconducting Gap in Semiconductor Majorana Nanowires. *Physical Review Letters* **110**, 186803 (2013).
25 Stanescu, T. D., Tewari, S., Sau, J. D. & Das Sarma, S. To Close or Not to Close: The Fate of the Superconducting Gap Across the Topological Quantum Phase Transition in Majorana-Carrying Semiconductor Nanowires. *Physical Review Letters* **109**, 266402 (2012).
26 Mishmash, R. V., Aasen, D., Higginbotham, A. P. & Alicea, J. Approaching a topological phase transition in Majorana nanowires. *Physical Review B* **93**, 245404 (2016).
27 Liu, C.-X., Setiawan, F., Sau, J. D. & Das Sarma, S. Phenomenology of the soft gap, zero-bias peak, and zero-mode splitting in ideal Majorana nanowires. *Physical Review B* **96**, 054520 (2017).
28 Liu, C.-X., Sau, J. D., Stanescu, T. D. & Das Sarma, S. Andreev bound states versus Majorana bound states in quantum dot-nanowire-superconductor hybrid structures: Trivial versus topological zero-bias conductance peaks. *Physical Review B* **96**, 075161 (2017).
29 Das Sarma, S., Sau, J. D. & Stanescu, T. D. Splitting of the zero-bias conductance peak as smoking gun evidence for the existence of the Majorana mode in a superconductor-semiconductor nanowire. *Physical Review B* **86**, 220506 (2012).
30 Setiawan, F., Liu, C.-X., Sau, J. D. & Das Sarma, S. Electron temperature and tunnel coupling dependence of zero-bias and almost-zero-bias conductance peaks in Majorana nanowires. *arXiv:1708.09039* (2017).

31 Kells, G., Meidan, D. & Brouwer, P. W. Near-zero-energy end states in topologically trivial spin-orbit coupled superconducting nanowires with a smooth confinement. *Physical Review B* **86**, 100503 (2012).
32 Lee, E. J. H. *et al.* Zero-Bias Anomaly in a Nanowire Quantum Dot Coupled to Superconductors. *Physical Review Letters* **109**, 186802 (2012).
33 Pikulin, D. I., Dahlhaus, J. P., Wimmer, M., Schomerus, H. & Beenakker, C. W. J. A zero-voltage conductance peak from weak antilocalization in a Majorana nanowire. *New Journal of Physics* **14**, 125011 (2012).
34 Stanescu, T. D. & Tewari, S. Disentangling Majorana fermions from topologically trivial low-energy states in semiconductor Majorana wires. *Physical Review B* **87**, 140504 (2013).

Acknowledgments We acknowledge stimulating discussions with Michael Wimmer and Önder Gül. This work has been supported by the European Research Council, the Dutch Organization for Scientific Research (NWO) and Microsoft Corporation Station-Q.

Author Contributions

The teams in Eindhoven and Santa Barbara have grown the nanowires with epitaxial Al and performed the nanowire deposition. The team in Delft fabricated the devices, performed electrical measurements, and analysed the experimental data. The Maryland team performed the numerical simulations. The manuscript was written by HZ and LPK with comments from all authors.

Method

Theory model. We use the theoretical model from reference 28 to perform numerical simulations with experimentally relevant parameters, such as the effective mass $m^* = 0.015\ m_e$, the spin-orbit coupling $\alpha = 0.5$ eVÅ, the chemical potential of the lead $\mu_{lead} = 25$ meV, the Landé g-factor $g = 20$ such that the Zeeman energy V_Z [meV] = 1.2 B [T], and the length of the nanowire $L = 1.0$ μm. Note that the collapse of the bulk Al superconducting gap is included explicitly in the theory to be consistent with the experimental situation where the bulk gap collapses ~ 1T.

Lorentzian fit. We fit our ZBP line-shape with the Lorentzian formula: $G(V) = \frac{2e^2}{h} \times \frac{\Gamma^2}{\Gamma^2+(eV)^2}$, where Γ defines the tunnel coupling and FWHM of the peak, i.e. 2Γ. Then we do convolution integration with the derivative of the Fermi distribution function (at 20 mK) to fit our ZBP shape. Since the FWHM of our ZBP is much larger than the thermal width, we took Γ to be roughly equal to half of the FWHM for all the fittings in Fig. 4c and Fig. 5f.

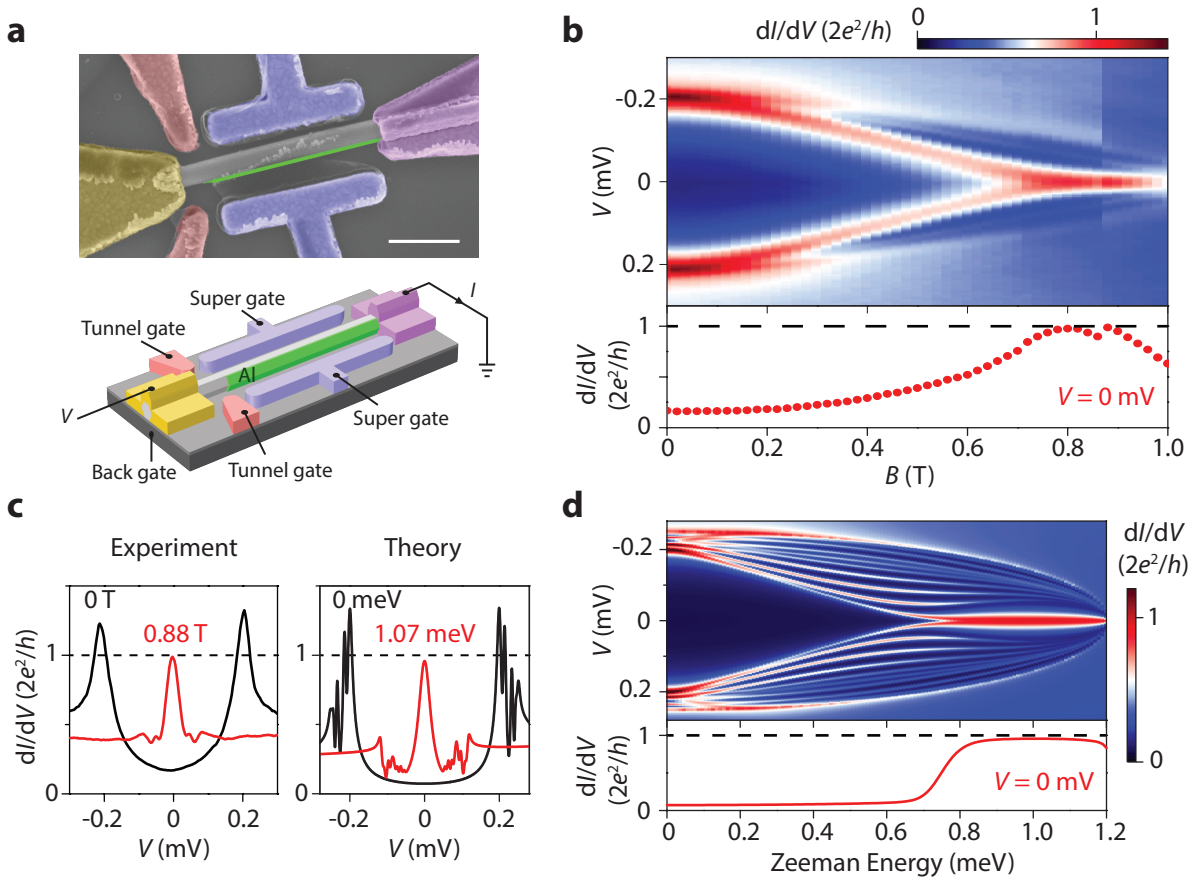

Figure 1: **Quantized Majorana zero bias peak**. **a** False-color scanning electron micrograph of device A (upper panel) and its schematics (lower panel). The scale bar is 500nm. Side gates and contacts are Cr/Au (10nm/100nm), labeled by different colors. The substrate is p-doped Si, acting as a global back gate, covered by 285nm SiO_2. The two tunnel (super) gates are short externally as one tunnel (super) gate. **b** Magnetic field dependence of the quantized ZBP with the zero bias line-cut in the lower panel. Magnetic field direction is aligned with the nanowire axis for all the measurement. Super (tunnel) gate voltage is fixed at -6.5V (-7.7V), while back gate is kept grounded. Temperature is 20mK unless specified. **c** Comparison between experiment and theory. Left (right) panel is the vertical line-cuts from **b** (**d**) at 0T and 0.88T (1.07meV). **d** Majorana simulation of Device A, qualitative agreeing with the experiment data. A small dissipation term ($\sim 30mK$) is introduced to account for the effect of finite temperature and small lock-in excitation voltage ($8\mu V$).

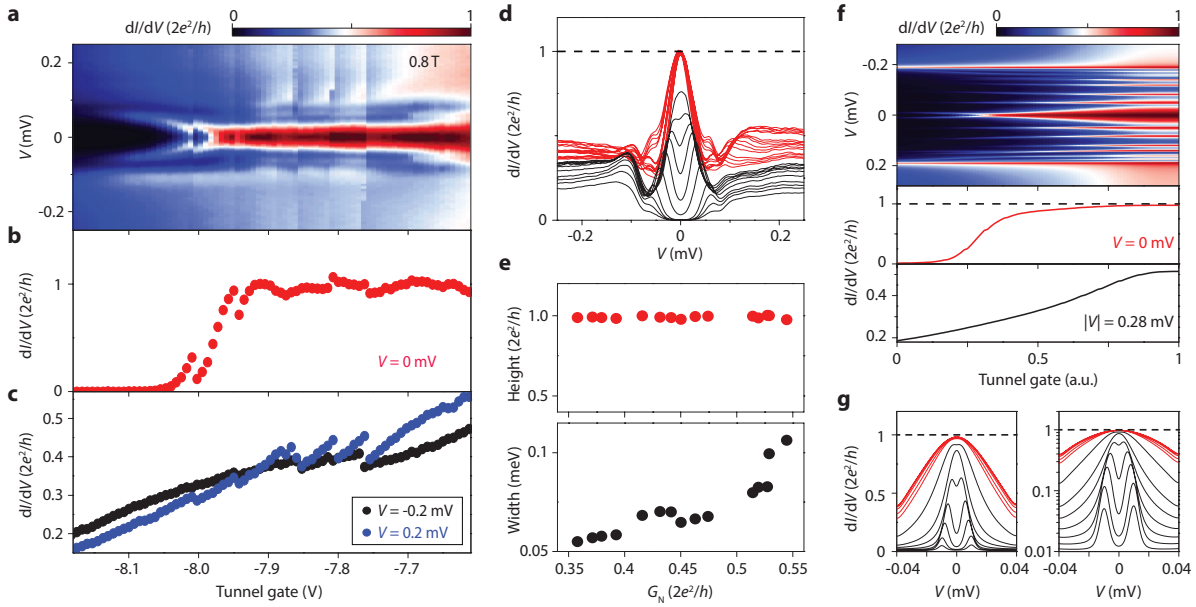

Figure 2: **Quantized Majorana conductance plateau**. **a** Tunnel gate dependence of the quantized ZBP at B=0.8T. Super (back) gate voltage is fixed at -6.5V (0V). The ZBP remains robust (un-split) with the tunnel gate voltage changing from -7.6V to -7.95V. Until the more negative tunnel gate voltage splits the ZBP. **b,c** Horizontal line-cuts from **a**, showing zero bias conductance and above-gap conductance, respectively. The above-gap conductance (transmission) changes from $0.35 \times 2e^2/h$ to $0.55 \times 2e^2/h$, while the ZBP height remains close to $2e^2/h$, i.e. a quantized plateau. **d** Several vertical line-cuts from **a**, showing quantized ZBP curves (red). The above-gap conductance is changed by more than 50%, while the ZBP height sticks at $2e^2/h$. The black curves show the zero bias conductance drops from the quantized value when the ZBP starts to split. **e** The ZBP peak height (red dots) and width (black dots) extracted from **d** (red curves), as a function of above-gap conductance(G_N). The width is defined by the bias voltage value at which the dI/dV is e^2/h. **f** Majorana simulation on the tunnel gate dependence, qualitatively agrees with the experiment data. **g** Vertical line-cuts from **f** in both linear and log scale showing the quantized ZBP (red) and split-peaks (black).

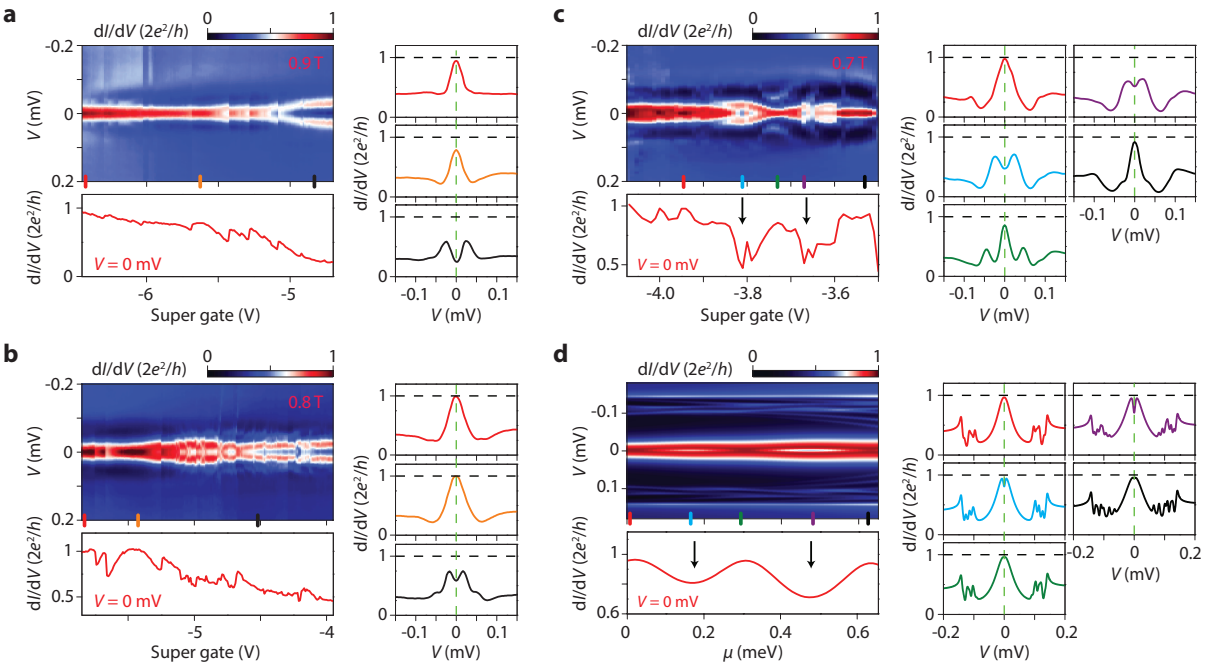

Figure 3: **Majorana splitting and oscillations. a-c** Super gate dependence of the quantized ZBP at difference fixed mangentic fields: 0.9T, 0.8T and 0.7T respectively. The tunnel gate voltage is adjusted simultaneously when sweeping the super gate voltage, to compensate for the cross coupling between the two gates. The transmission (above-gap conductance) is kept roughly as a constant. The super gate mainly tunes the chemical potential in the proximitized nanowire part. Lower panel is the zero bias line-cut, while the right panel shows vertical line-cuts at gate voltages indicated by the corresponding color bars. The ZBP remains unsplit over a large super gate voltage range, with its peak height close to $2e^2/h$. More positive super gate voltage increases the chemical potential, which splits the ZBP by driving the system from topological into trivial regime. Switches in the color maps are due to charge jumps in the gate dielectric. **c** shows oscillatory behavior of the ZBP, i.e. increasing the super gate voltage gives a ZBP-split peak-ZBP-split peak-ZBP pattern, as clearly shown in the line-cuts. The two split peak regions correspond to the two valleys in the zero bias line-cut (indicated by the back arrows). This could be explained by the oscillation of Majorana wavefunciton overlaping, as shown in **d**. **d** Theory simulation of Majorana conductance showing oscillatory splitting behavior as a function of chemical potential.

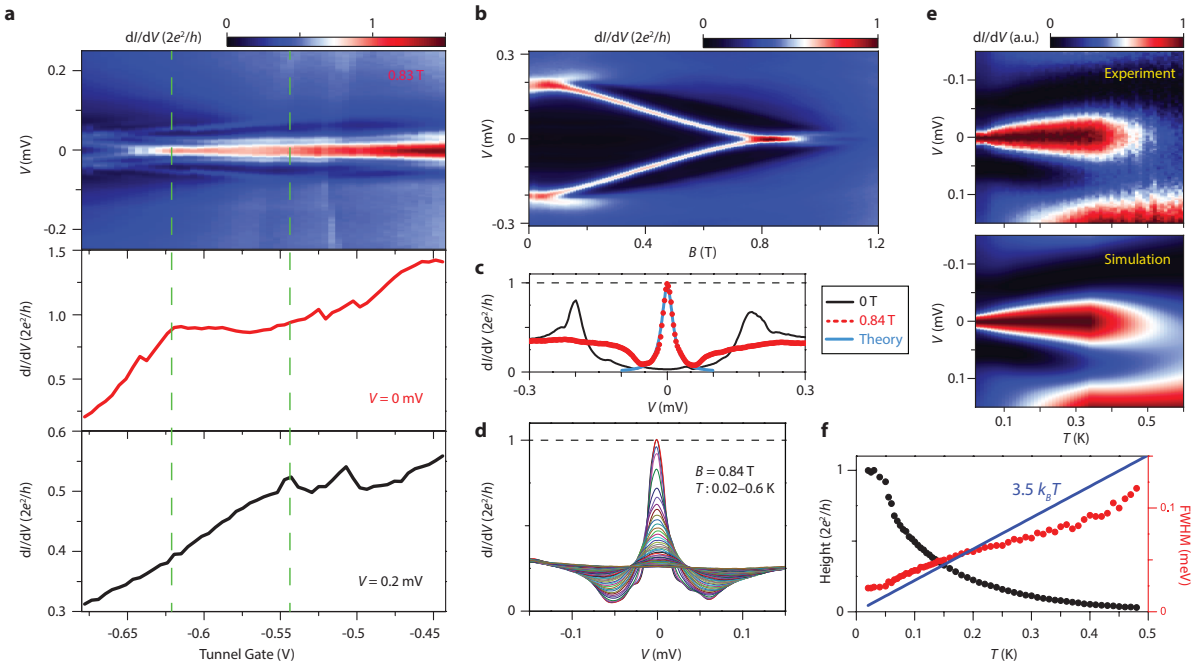

Figure 4: **Majorana plateau reproduced, and its temperature dependence**. **a** Tunnel gate dependence of the ZBP in Device B at B=0.83T. For tunnel gate voltage between -0.62V and -0.54V (the two green dashed lines), the above-gap conductance changes from $0.8 \times e^2/h$ to $1.06 \times e^2/h$, by 33%. In the meantime, the ZBP height remains constant at $\sim 0.9 \times 2e^2/h$, resolving a plateau close to the quantized value. More positive gate voltage pushes the zero bias conductance exceeding $2e^2/h$, due to the increase of background, contributed by other populated channels. After the right green dashed line, the above-gap conductance is larger than e^2/h, meaning more than one channel is populated. The net ZBP height (after subtracting background) never exceeds $2e^2/h$. **b** Magnetic field dependence of the quantized ZBP. **c** Vertical line-cuts from **b** at 0T and 0.84T. The ZBP line-shape fits quite well with the Majorana theory (blue line), by assuming a tunnel coupling $\Gamma = 13.7\mu eV$ and temperature of 20mK. **d** Temperature dependence of this quantized ZBP with temperature varies from 20mK to 600mK with 10mK step. **e** Color plot of the temperature dependence in **d**. At each temperature the conductance is renomalized for clarity by setting the minimum 0 and maximum 1. As the temperature increases, the ZBP is thermal broadened and smeared out at ~500mK. Lower panel is the theory simulation, agreeing perfectly well with the experiment. **f** ZBP height and FWHM as a function of temperature (extracted from **e**). As the temperature decreases, the ZBP height saturates at $2e^2/h$, while the ZBP width becomes wider than thermal broadening (above the $3.5k_BT$ blue line). See Extended data for more information.

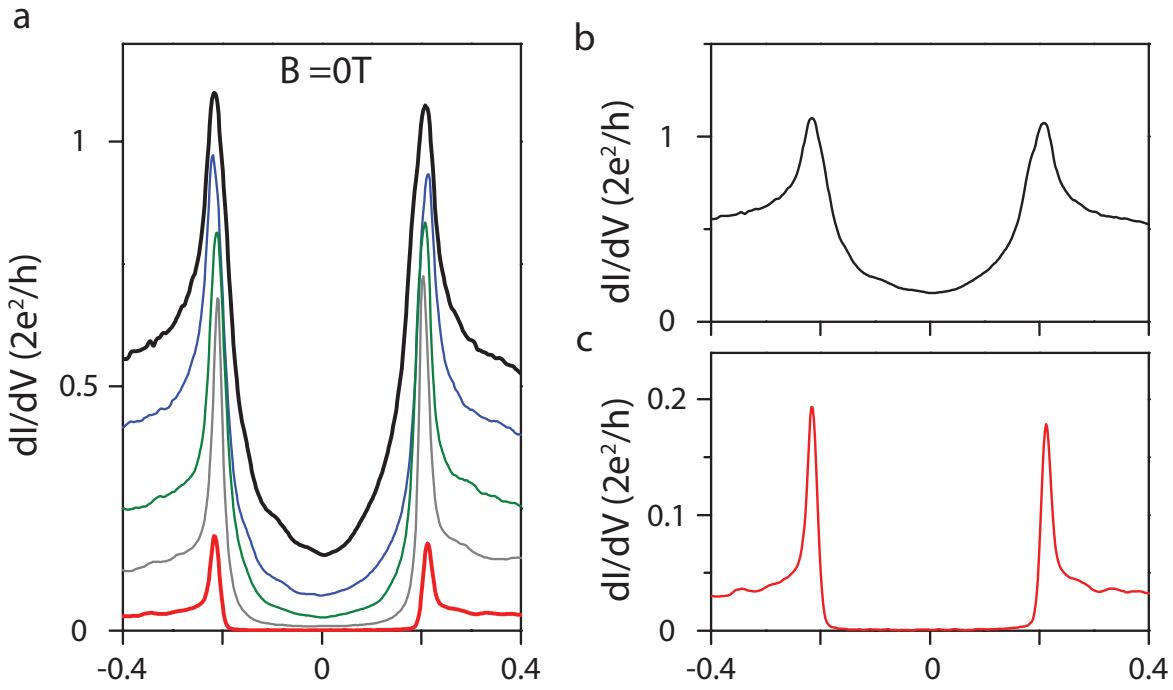

Extended Data Figure 1 | Dissipationless 'soft gap' due to large Andreev reflection. a dI/dV of Device A as a function bias voltage. Different curves are for different fixed tunnel gate voltages (transmissions). In the deep tunneling regime (red curve), where the above-gap conductance ($\sim 0.03 \times 2e^2/h$) is much less than $2e^2/h$, dI/dV is proportional to the density of states in the proximitized wire part, resolving a hard superconducting gap. In the open regime (black curve), where the above-gap conductance (transmission) is comparable with $2e^2/h$ (unity), the sub-gap conductance is non-zero, reminiscent of soft gap. But the finite sub-gap conductance is contributed by Andreev reflection, instead of dissipation (a real soft gap). This fake soft gap does not affect the quantized ZBP height. **b** Re-plot of the two curves from **a**.

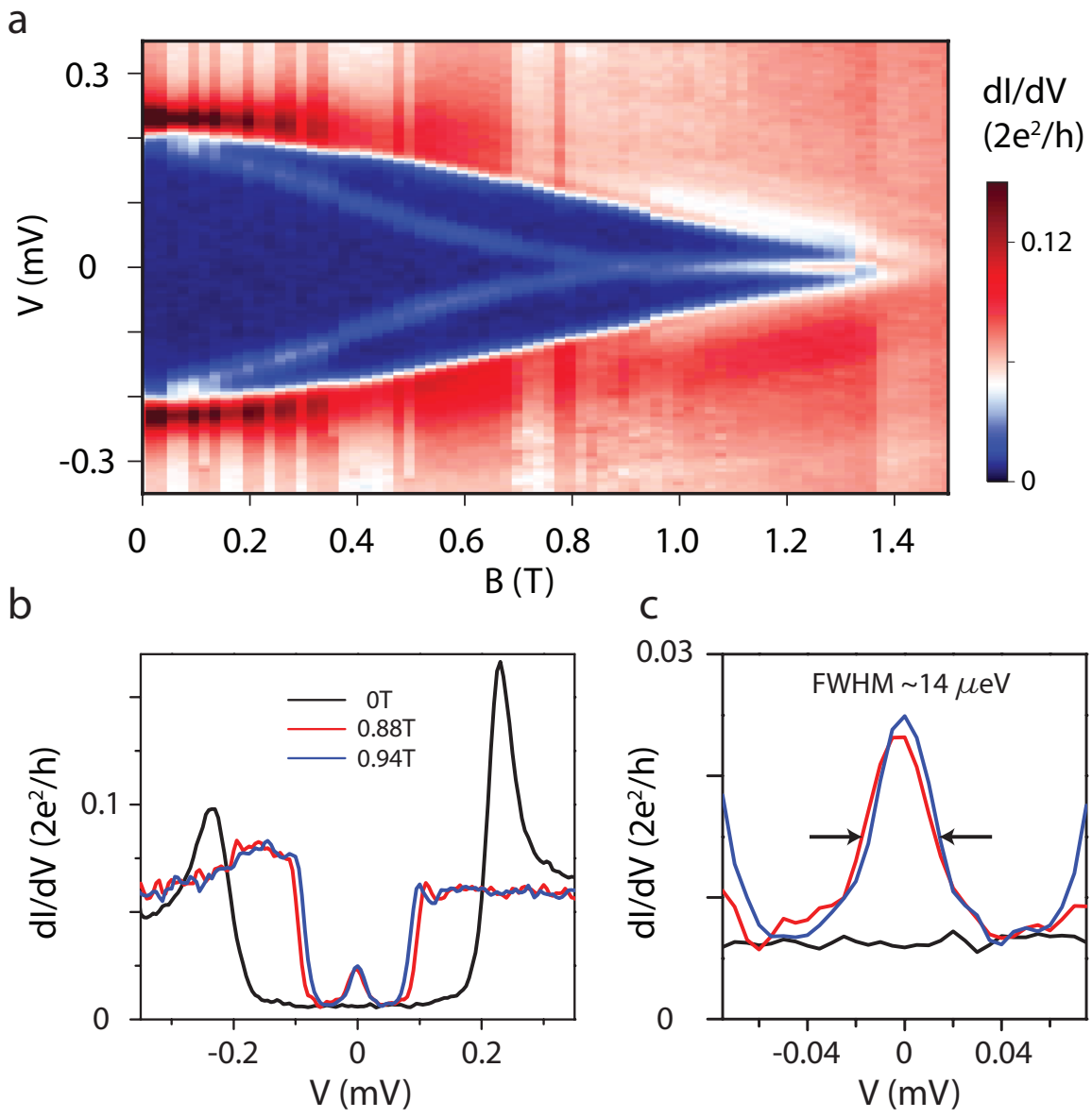

Extended Data Figure 2 | Thermal broadened low ZBP coexists with hard gap. a dI/dV of device C, as a function of magnetic field, resolving a stable ZBP. **b** Vertical line-cuts from **a**, at three different magnetic fields. At B=0T, the above-gap conductance ($\sim 0.05 \times 2e^2/h$) is much less than $2e^2/h$ (deep tunneling regime), resolving a hard gap. The residue sub-gap conductance is due to the small Andreev reflection and noise background from the measurement equipment. The small transmission leads to a narrow width of the ZBP, whose height is greatly affected (decreased) by thermal broadening. The sub-gap conductance at the finite magnetic field where ZBP exists, is the same with the sug-gap conductance at zero field, suggesting that the gap remains hard at the magnetic field where we create Majoranas. **c** A zoom-in image shows the FWHM of the ZBP is $\sim 14\mu eV$, consistent with the sum of the thermal broadening width ($3.5k_BT$, $6\mu eV$ at 20mK), the lock-in bias voltage excitation ($5\mu eV$) and the original peak width at T=0K.

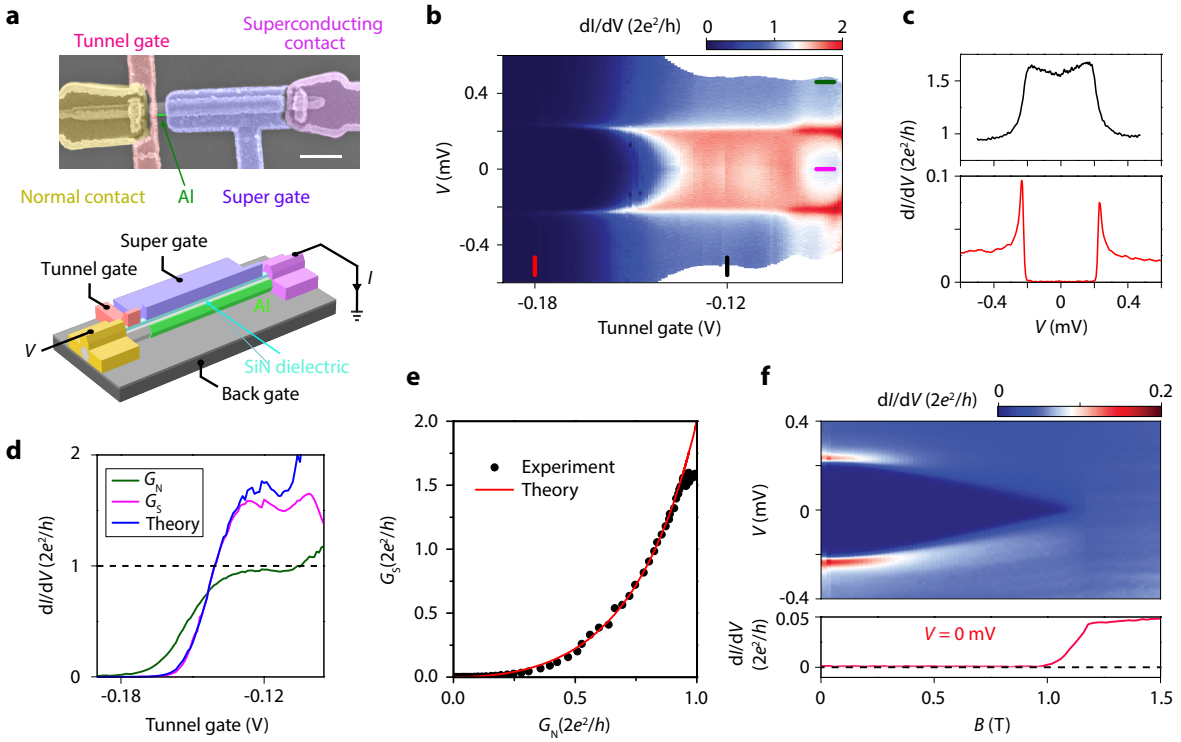

Extended Data Figure 3 | Perfect ballistic Andreev transport in InSb-Al nanowires. a False-color scanning electron micrograph of device D. The scale bar is 500nm. Electrical contacts and top gates are Cr/Au and labeled with different colors. Lower panel shows the device schematic and measurement set up. The two top gates (tunnel gate and super gate) are separated from the nanowire by 30nm thick SiN dielectric. The global back gate is p-dopes Si covered by 285nm thick SiO_2 dielectric. **b** Differential conductance (dI/dV) of Device D, as a function of bias voltage (V) and tunnel gate voltage. **c** Vertical line-cuts from **b** at tunnel gate voltage = -0.18V (lower panel) and -0.12V (upper panel), resolving hard superconducting gap in the tunneling regime (lower panel) and strong Andreev enhancement on the plateau (upper panel). **d** Horizontal line-cuts from **c** for V=0mV (pink, sub-gap conductance, G_S) and V=0.45mV (green, above-gap conductance, G_N). The blue curve is the calculated sub-gap conductance using $G_S = 4e^2/h \times T^2/(2-T)^2$, where transmission T is extracted from the above-gap conductance: $G_N = 2e^2/h \times T$. **e** G_S as a function of G_N (black dots) and its comparison with the theory fit: $G_S = 2 * G_N^2/(2 - G_N)^2$, with G_S and G_N in unit of $2e^2/h$. **f** Magnetic field dependence of the hard gap. Lower panel shows the zero bias line-cut. The gap remains hard until 1 Tesla where the superconducting gap closes.

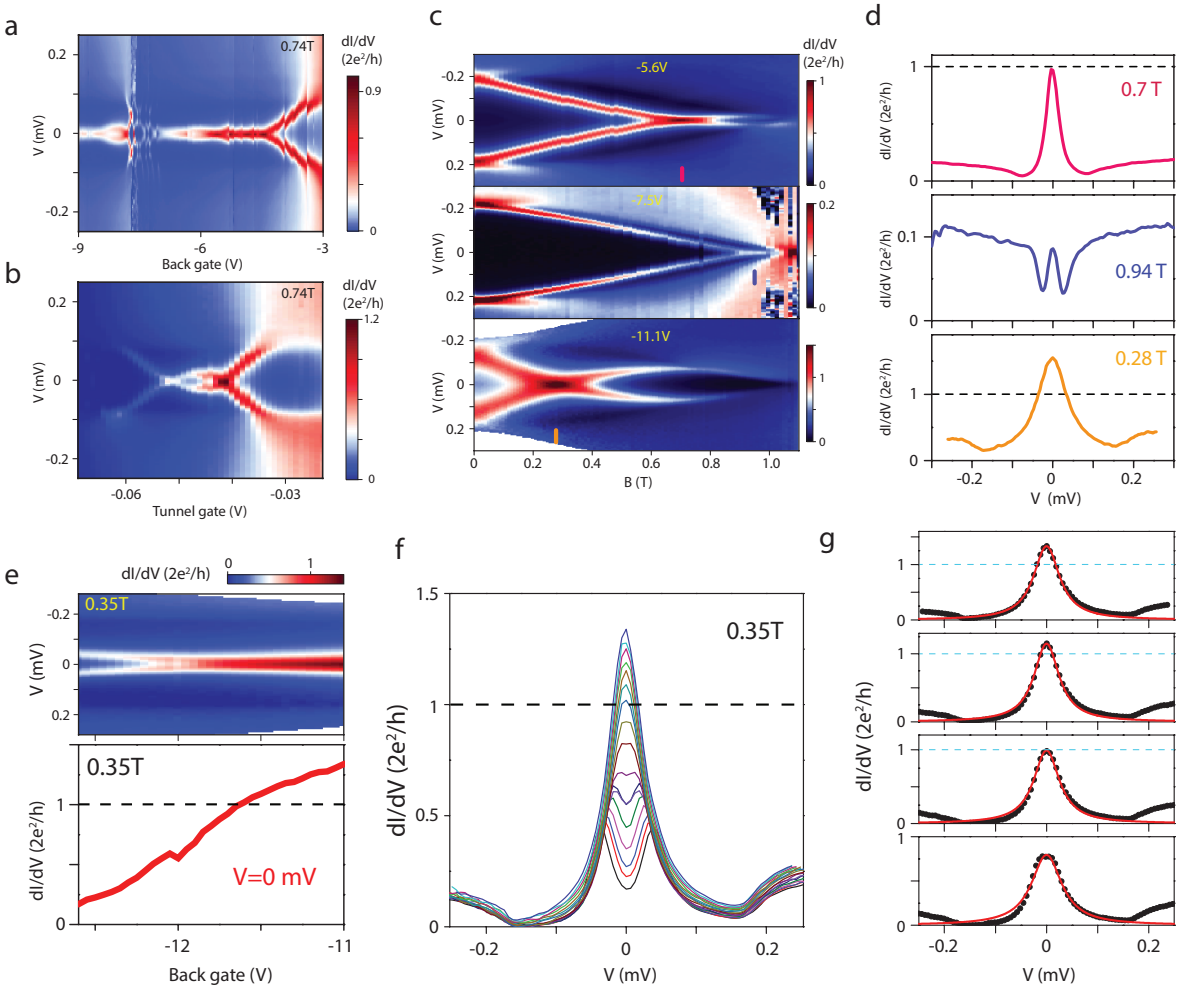

Extended Data Figure 4 | Trivial zero bias peaks from Andreev bound states. a dI/dV of Device D, as a function of back gate voltage which tunes the chemical potential in the proximitized wire part. Tunnel and super gate voltages are fixed at -0.03V and 0V, respectively. B=0.74T. **b** Tunnel gate dependence of this ZBP. The super and back gate voltages are fixed at 0V and −5.6V, respectively. B=0.74T. The zero bias peak does not remains stable (un-split) over tunnel gate voltage change, and only exists at the crossing points of the Andreev levels. This indicates that the ZBP has a trivial origin which is from Andreev bound states localized near the tunnel barrier due to the potential fluctuations there. Thus the tunnel gate voltage change can modify the potential fluctuations, chaning the Andreev bound state energy. **c** Magnetic field dependence of this trivial ZBP at different back gate voltages (-5.6V, -7.5V and -11.1V). The tunnel (super) gate voltages are -0.05V (0.05V), -0.05V (0.05V) and 0.01V (-0.44V), respectively. **d** line-cuts of the ZBPs from **c**, showing the trivial ZBP height varies with different gate setting. It can be exactly at $2e^2/h$, or much less (larger) than this quantized value. **e** Back gate dependence of the ZBP at 0.35T, for tunnel and super gate voltages fixed at 0.01V and 0V, respectively. Lower panel shows the zero bias line-cut, where the zero bias conductance continues to increase across $2e^2/h$. **f** Vertical line-cuts from **e** (with only half the lines plotted for clarity), showing a continuous change of zero bias peak height. This trivial ZBP height continuously varies with gate voltage change and does not resolve a plateau like the Majorana case (Figure2 and Figure 4). **g** Lorentzian fit (red curve) of the trivial ZBPs (black dots) taken from **f**. We assumed a temperature broadening of 20mK. This Lorentzian fit applied equally well for trivial ZBPs here and the Majorana case in Figure 4c. This means that the ZBP shape can not be used to distinguish Majoranas from ABS.

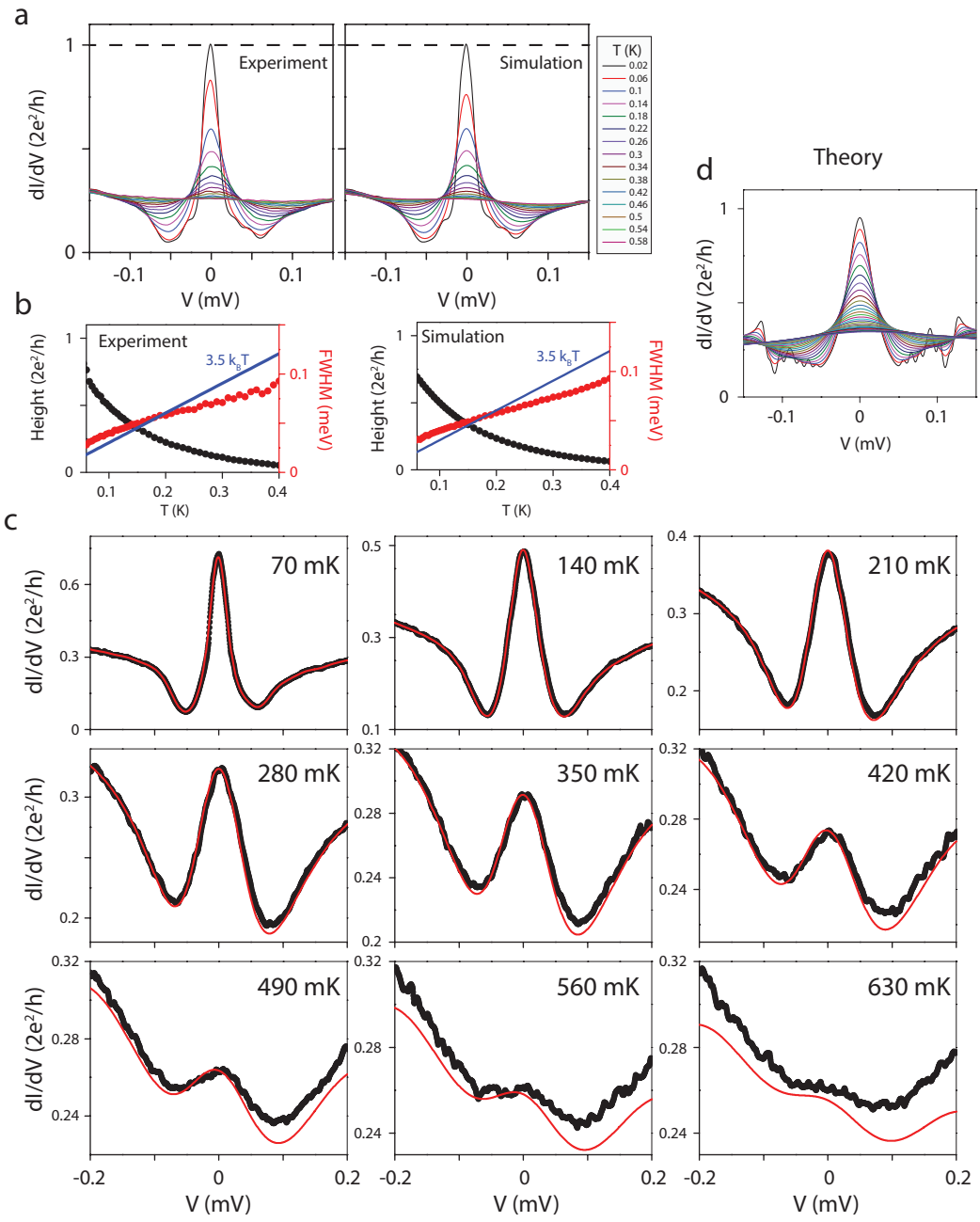

Extended Data Figure 5 | Temperature dependence simulation of the quantized Majorana zero bias peak in Device B. We take the dI/dV curve at 20mK as the input, and assume this as the zero temperature dI/dV. Then we perform the convolution of the derivative of Fermi distribution function to calculate the $dI/dV = G(V,T) = \int_{-\infty}^{\infty} d\epsilon G(\epsilon,0)\frac{df(eV-\epsilon,T)}{d\epsilon}$ at any temperature T and bias voltage V, $f(E,T)$ is the Fermi function. Because we use 20mK data as the zero temperature data, our model only works for T sufficiently larger than 20mK, e.g. $(T > 50mK)$. **a** Comparison of the experimental data (left, taken from Fig.4d) and theory simulations, for different temperatures. **b** Comparison of the extracted peak height and width as a function of temperature between experiment (left panel, taken from Fig.4f) and theory simulations (right panel). **c** Several typical curves at different temperatures, black dots are the experimental data while the red curves are the theory simulations. The perfect agreement between simulation and experiment indicates that thermal averaging effect is the dominating effect that smears out our Majorana ZBP in our temperature dependence. **d** Temperature dependence of the theory simulated zero bias peak take from Figure 1c (right panel). The temperature is from 25mK to 700mK with 23 mK step.